Optical properties of gallium selenide under high pressure

M. Gauthier, A. Polian, J. M. Besson, and A. Chevy
Physique des Milieux Condensés, Tour 13, 4e Etage, Université Pierre et Marie Curie, 4 place Jussieu, F-75252 Paris CEDEX 05, France
(Received 10 March 1989)

Compressibility, optical-absorption, Raman-scattering, and refractive-index measurements for GaSe are reported at 300 K and pressures up to 8 GPa. A model which separates intra- and interlayer contributions along the c axis is used, with adequate deformation potentials, to quantitatively reproduce the compressibility along the c axis, the refractive-index variation, and the shift of both direct and indirect gaps under pressure. The shape of the absorption edges are calculated by the Elliott-Toyozawa formalism at all pressures, between 1.6 and 2.4 eV, with only one constant, and two pressure-dependent parameters: the exciton Rydberg and the matrix element for the direct transition. The decrease of the former, together with the measured shift of the TO and LO modes are interpreted by a large increase of the longitudinal effective charge under pressure which can be assigned to either intralayer-to-interlayer charge transfer, or to an increase of the total ionicity, or both.

I. INTRODUCTION

The study of anisotropic crystals is of interest due to the differences in the various kinds of interactions between their constituent atoms. The use of the pressure parameter is particularly powerful since it allows one to vary the ratio of the interactions, and thus helps in identifying the nature of the interactions involved in the various physical properties. In this respect, gallium selenide is a choice model. It is a layered semiconductor of the III-VI family, like GaS or InSe. The basic units, two-dimensional layers, are formed by two hexagonal sheets with gallium and selenium atoms at alternate corners of the hexagons; the hexagonal layers undergo "chairlike" deformation through bonding of the gallium atoms by a strong ionicovalent bond. At ambient, the layers are bound by weak van der Waals–type interactions. The weakness of this interaction explains the existence of a number of polytypes.[1–5] In the most common one, called ε, there are two layers, i.e., eight atoms in the unit cell, and the crystal belongs to the D^1_{3h} space group.

The room-temperature physical properties of GaSe are reasonably well known. Under pressure, several experimental studies have already been performed, like Raman scattering[6–8] or transmission measurements.[9–15] These experiments show that the band gap that lies in the visible range at room pressure ($E_g = 2.02$ eV) shifts toward lower energies when pressure is applied. This has been recently interpreted[15] using adequate deformation potentials, to fit the absorption curves in the vicinity of the absorption edge, and then extract the variation of the direct band gap up to 2 GPa. Since the compressibility of GaSe along the c axis was not measured, the corresponding value for InSe was used in this work. As will be shown here, the compressibility of InSe along the c axis is actually 50% smaller than that of GaSe at low ($P < 4$ GPa) pressures. For this reason, this analysis fails to account for the band-gaps variation above 2 GPa. Moreover, the absorption edge is quantitatively reproduced only 50 meV above and below the direct-gap energy.

In the present paper we present a set of measurements which allows us to complete the pressure dependence of both direct and indirect band gaps up to 8 GPa over an energy range of about 1 eV around the direct-gap energy. First, we measure the compressibility along the c axis and fit it with a simple model which separates the intra- and the interlayer contributions. Then, the refractive index is determined by an interferometric technique up to 8 GPa that gives results in agreement with those of Kuroda *et al.*[8] The absorption coefficient and finally the Raman-scattering spectrum are measured up to 8 GPa. Over this pressure range this set of results allows us to analyze and reproduce the refractive-index variation, and the absorption coefficient spectrum of GaSe between 1.5 and 2.4 eV. The calculations are performed in the framework of the Elliott-Toyozawa theory, using contributions from direct and indirect processes, and taking into account the nonparabolicity of the energy bands. The deformation potentials that govern the pressure dependence of the gaps are determined. Finally, the absorption curves are reproduced with only one constant and two independent parameters, which are the Rydberg of the exciton and the matrix element of the direct transition versus pressure. The pressure dependence of these two parameters is then explained in terms of charge transfer from the intra- to the interlayer bonds, and evolution of the band structure under pressure.

Section II is devoted to the description of the experimental procedures. The results are given in Sec. III and discussed in the last section.

II. EXPERIMENT

In all experiments the samples used were grown in our laboratory, either by vapor transport or by the Bridgman

method.[16] We used both hexagonal needles of γ and ε polytypes with natural faces parallel to the c axis or thin slabs with natural faces perpendicular to the c axis.

Four kinds of measurements were done under high pressure, i.e., compressibility, refractive index, Raman scattering, and transmittancy.

The pressure was generated by a classical Block and Piermarini diamond-anvil cell[17,18] (DAC). The sample ($150\times150\times25$ μm^3) is placed together with a ruby chip in a 300-μm-diam hole drilled in a 60-μm-thick Inconel X750 gasket and inserted between the diamonds of the DAC. Before closure of the DAC, the hole is filled with the classical 4:1 methanol-ethanol mixture to ensure nearly hydrostatic conditions up to 30 GPa.[19,20]

The pressure is derived from the shift of the R_1 line of the ruby fluorescence using the linear law[17]

$$P=\frac{\lambda(P)-\lambda(P=0)}{\lambda} \quad \text{with } A=3.63 \text{ Å/GPa} .$$

The difference with more recent polynomial laws[21] is only 1.5% at 20 GPa, which is the maximum pressure reached in our experiments.

A. Compressibility along the c axis

We have measured the relative variation in length of as-grown oriented needles with the c axis perpendicular to the optical axis of the DAC. All the data are taken on increasing pressure using a microphotographic method described earlier[22] to get $c(P)$. At each pressure, we take microphotographs of the sample in the DAC at constant magnification ($\times400$). The length of the sample image can thus be plotted versus pressure.

We have verified that no systematic error, coming, for example, from a lensing effect due to the deformation of the anvils of the cells, is involved up to 25 GPa by comparing the known equation of state of diamond with results obtained in this way, on a thin (25 μm) diamond slab placed in the cell.

From systematic measurements at the same pressure and from the scatter of data obtained in the experiment on diamond, the standard random error is estimated to be ±0.6 μm. This leads to a relative error $\Delta c/c$ of about 0.6% with an initial sample length of 102 μm, although the actual dispersion (Fig. 1) is much lower.

B. Optical constants

All the experiments reported thereafter have been done in the E⊥c geometry with the incident light parallel to the c axis and, thus, the electric field vector **E** perpendicular to **c**. We have used thin slabs with thicknesses of the order of 25 μm.

1. Refractive index

The property of layer compounds to give good plane parallel faces by cleaving allows us to determine the refractive index by an interferometric method. One only gets the optical path length, ne, from the interference pattern by the relation

$$2ne=k\lambda , \tag{1}$$

where k is the interference order, e the thickness of the sample, and n the refractive index at wavelength λ in the E⊥c geometry: n will thus refer to $n_\perp$ throughout this section.

At ambient pressure we used previously published data for $n(\lambda)$,[23,24] and we determined both the thickness of the sample and the interference order k at a given wavelength.

From our measurements, the variation of $e(P)$ is known (Sec. II A) and thus we can follow a given interference order k versus pressure, and finally Eq. (1) allows us to determine $n(\lambda,P)$ with a precision better than 1%.

2. Transmittancy

The absorption coefficient was measured in the DAC up to 8 GPa. At higher pressures the absorption onset is outside the spectral range of our spectrometer (1.5–2.7 eV).

The transmittancy I/I_0 was measured by the sample-in–sample-out method: I is the intensity transmitted through the sample, and I_0, the incident intensity, is measured through the pressure-transmitting medium in the cell, near the sample, by moving the DAC perpendicular to the beam. In order to prevent errors due to light diffusion in the cell, we used a two-pinhole system. The first one is used to make a small light spot in the cell ($\Phi\approx50$ μm). The second one, placed between the cell and the spectrometer, ensures that only light coming directly from the central part of the spot area is analyzed. This method reduces the stray-light $T_{\min}$ down to 8.0×10^{-4}, so that transmittancies as low as 10^{-3} can be measured after stray-light corrections.

At low energy, far below the absorption edge of the sample, a nonzero and constant value for the apparent absorption coefficient is found. This is a general case in optical measurements on transparent crystal samples and results owing to various reasons: imperfections of the crystal, diffusion at the interfaces, etc. In the low-frequency region, where GaSe is known to be transparent, the apparent transmittancy is corrected by a constant factor a to fit the theoretical transmittancy for $\alpha=0$. This factor is experimentally determined for each pressure and sample by measuring the low-energy, constant-transmittancy region.

Finally, the absorption coefficient α is given by

$$\alpha=\frac{1}{e}\ln[X+(X^2+R^2)^{1/2}] ,$$

with

$$X=\frac{1-R^2}{2a(T-T_{\min})}$$

and

$$R=\left[\frac{n-n_0}{n+n_0}\right]^2 ,$$

where n is the refractive index of GaSe, n_0 the refractive

index of the methanol-ethanol pressure-transmitting medium, T the experimental transmittancy, a the correction factor, and e the thickness of the sample. It should be noted that the correction due to the stray light ($T_{\min}$) has been taken into account in the high-energy, low-transmittancy region.

The refractive index of the methanol-ethanol mixture $n_0(P)$ has been extrapolated from the results of Vedam *et al.*[25] with the Clausius-Mossotti law:

$$3\frac{n_0^2-1}{n_0^2+2}=A\rho\ ,$$

with $A=0.755\times10^{-3}$ m^3kg^{-1} and ρ the density in $kg\,m^{-3}$. The variation of density is known only up to 6 GPa for methanol and ethanol.[26] We used a first-order Murnaghan equation of state (EOS) (Refs. 27 and 28) to extrapolate the results up to 8 GPa with $B_0=2$ GPa and $B_0'=7.1$.

Final errors in the absorption coefficient α due to errors in the determination of the refractive index of the methanol-ethanol mixture and GaSe and in the experimental transmittancy are less than 2% for $100<\alpha<2500$ cm^{-1}, these limits being set by the thickness of the sample.

C. Raman scattering

Raman-scattering measurements were done on the ε and γ polytypes of GaSe. We used a backscattering geometry $Z(--)\bar{Z}$ with the incident light parallel to the c axis of the sample.

Spectra were recorded with a 2.4-m-focal-length triple monochromator with a cooled photomultiplier detector and a photon-counting system. The spectral resolution of the system is better than 0.8 cm^{-1} at 755 nm with a slit width of 150 μm.

Because of the red shift of the optical edge of GaSe under pressure,[29] it has been shown[6–8] that Raman scattering on GaSe requires near-infrared-wavelength excitation under high pressure. We used the 755-nm line (1.642 eV) of a krypton laser with an incident power of 50 mW on the sample to avoid excessive absorption and heating of the sample. With this wavelength, reliable data could be obtained only up to 6 GPa.

No deconvolution has been done on the experimental spectra. Instrumental response is included in the width at half maximum given for the Raman modes.

III. RESULTS

A. Compressibility along the c axis

The ratio of the length of the sample along the c axis at pressure P to the length at ambient pressure $c(P)/c(0)$ versus pressure is shown in Fig. 1. We do not observe any phase transition either near 0.5 GPa (Ref. 11) due to a polytypic transformation as in GaS (Refs. 30–32) or near 6 GPa (Ref. 6) due to the transition to a three-dimensional network as in InSe.[33,34] Here, within the precision of our measurements, no evidence for a phase transition could be obtained, this being confirmed by our Raman-scattering results and refractive-index values reported thereafter. Therefore, the $c(P)$ behavior is interpreted as a continuous variation in the ε phase of GaSe.

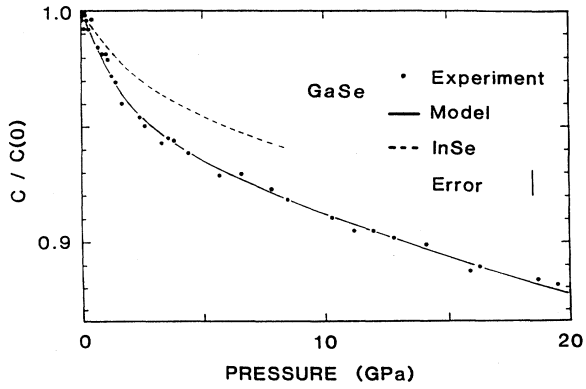

FIG. 1. Variation of length of an oriented needle of GaSe vs pressure. The solid line is obtained via a modified Murnaghan EOS (see text). The dashed line is the EOS of InSe previously used for calculations on GaSe (Ref. 15). To first order, GaSe and InSe are very similar: InSe is much harder and is only the high-pressure version of GaSe. Coincidence of the InSe and GaSe EOS's for $c(P)$ can be obtained by comparing the InSe behavior with that of GaSe shifted up by 0.85 GPa. The error bar is an estimate on the absolute error on Δc. Note that the actual scatter of points is much lower.

Below 3 GPa the linear compressibility along the c axis, χ_c, decreases very rapidly, whereas at high pressure ($P>5$ GPa) it is almost pressure independent and of the same order of magnitude as χ_a,[22] the linear compressibility perpendicular to the c axis. This shows that the lamellar behavior has to be taken into account. We used a modified Murnaghan EOS to reproduce the volume variation of GaSe under pressure.

The Murnaghan EOS is only valid for isotropic crystals.[27,28] We have included the anisotropy of GaSe by use of three "linear moduli" B_j, one per crystallographic direction j.

Crystallographic parameters l_j are solutions of the equations

$$\frac{dl_j}{l_j}=-\frac{dp}{B_j(P)}\ . \tag{2}$$

In the c direction the difference between interlayer van der Waals and intralayer covalent forces dominates the behavior of the crystal. GaSe can be modeled as an assembly of hard planes of compressibility χ_ℓ and thickness c_ℓ, where c_ℓ is the distance along the c axis between the Se sites in a layer, separated by a soft medium of compressibility χ_i, the van der Waals gap, and thickness c_i (Fig. 2). This has been clearly seen in the x-ray-diffraction experiments done on GaS (Refs. 30 and 32) under pressure. The Ga-Ga and Ga-S distances in the layer were shown to vary more slowly than the S-S distance between layers.

In a first approximation, the compressibility of a layer χ_ℓ is considered to be isotropic and constant with pres-

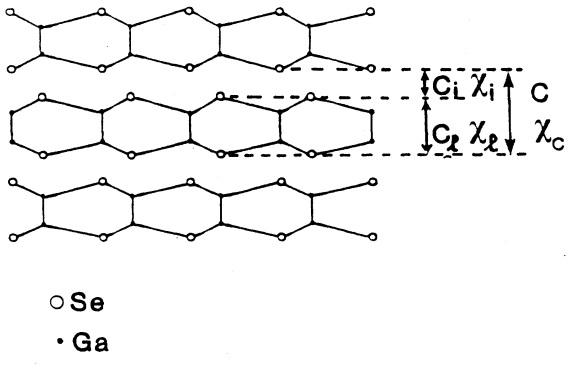

FIG. 2. Lamellar structure of GaSe modeled as hard isotropic planes of thickness c_ℓ and compressibility χ_ℓ separated by a soft medium, the van der Waals gap of thickness c_i, and compressibility χ_i. c_ℓ is the effective distance between the selenium atoms within a layer in the c direction, and c_i is the projection in the c direction of the distance between the selenium atoms of adjacent layers. The total thickness per layer, c, does not depend on the polytype. The macroscopic compressibility χ_c in the c direction is then related to χ_i,χ_ℓ and c_i,c_ℓ (see text).

sure as in GaS,[22,30,32] i.e., $\chi_\ell=\chi_a$.

The compressibility of the van der Waals gap, on the contrary, drastically changes with pressure. Following the Murnaghan model, its pressure dependence has to be taken into account.

Finally, with this simple model we have to solve Eqs. (2)–(6):

$$c(P)=c_\ell(P)+c_i(P) , \tag{3}$$

$$c\chi_c=c_\ell\chi_\ell+c_i\chi_i , \tag{4}$$

$$1/\chi_\ell=B_\ell(P)=B_{0\ell} , \tag{5}$$

$$1/\chi_i=B_i(P)=B_{0i}+B'_{0i}P+B''_{0i}P^2 , \tag{6}$$

where χ_c is the compressibility of GaSe in the c direction, $B_{0\ell}$ the linear rigidity of the layer, B_{0i} the linear rigidity of the van der Waals gap at atmospheric pressure, and B'_{0i} and B''_0 its pressure derivatives. Finally, we get

$$c_\ell=c_\ell(0)e^{-P/B_{0\ell}} , \tag{7}$$

$$c_i=c_i(0)\exp\left[-\frac{2}{Q}\tan^{-1}\left[\frac{Qp}{2B_{0i}+B'_{0i}P}\right]\right] , \tag{8}$$

with

$$Q=(4B_{0i}B''_{0i}-B'^2_{0i})^{1/2} .$$

The crystallographic parameters are known at room pressure for the γ polytype.[2,3] They are the same for the other polytypes if we normalize their thickness to one layer per cell.[1,4,5] So we used $c(0)=7.955$ Å, $c_i(0)=3.20$ Å, and $c_\ell(0)=4.755$ Å. A least-squares fit of the experimental $e(P)$ results gives the four parameters of the model:

$$B_{0\ell}=166.0\pm5.0 \text{ GPa} ,$$

$$B_{0i}=17.0\pm0.5 \text{ GPa} ,$$

$$B'_{0i}\approx0.25 ,$$

$$B''_{0i}\approx5.8 \text{ GPa}^{-1} .$$

This is very close to the extrapolation we can do from previous data[22,35–40] ($B_c\approx39$–40 GPa, $B_a\approx190$–200 GPa), which gives $B_{0\ell}\approx195\pm5$ GPa and $B_{0i}\approx17\pm1$ GPa. Moreover, the ratio $B_{0\ell}$ (or B_a)$/B_{0i}\approx10$–12 is in good agreement with the expected value from the force-constant models[31,40–43] that lead to a ratio of 10–20.

It should be emphasized here that the absolute values of B'_{0i} and B''_{0i} have no particular physical significance: here we just give the best-fit values. The fit is very insensitive to B'_{0i}, which may indeed be taken to be 2.0 instead of 0.2. The dominant term in $B_i(P)$ is B''_{0i}, which always remains very large ($4<B''_{0i}<6$). This is in contrast with van der Waals media, where the B' term is usually close to 7, and B'' can be neglected. Here, even with $B'_{0i}\approx\frac{7}{3}\approx2.3$, we still find $B''_{0i}>4$. This is an indication that the interlayer space is not a simple van der Waals gap under pressure and that interlayer bonds increase much faster (nonlinearly) with pressure. This will be utilized later in the discussion on intra- to interlayer charge transfer.

The difference between B_ℓ, the rigidity of the layer along the c axis, and B_a, the rigidity perpendicular to the c axis, is not significant. It can be due either to an incorrect definition of c_i and c_ℓ, or to the isotropic layer hypothesis, which is surely not exactly verified at very high pressure, or even to the fact that we have chosen to keep χ_a (the compressibility perpendicular to the c axis) pressure independent in a first approximation.

B. Optical constants

1. *Refractive index*

Figure 3 shows the relative variation of the optical path $ne(P)$ at two different energies: 1.5 eV (826.5 nm)

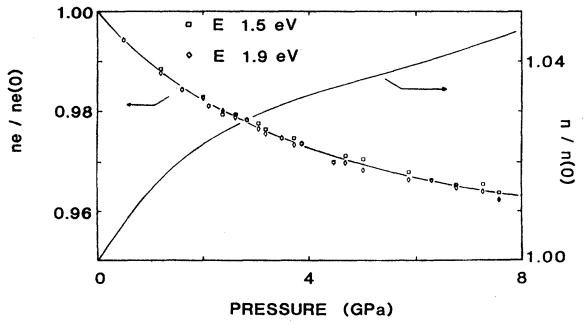

FIG. 3. Variation of the optical path ne and of the refractive index n vs pressure. Left-hand scale: relative variation of ne at two different energies. Right-hand scale: relative variation of the refractive index deduced from our EOS. The solid lines are calculated using the one-electron scheme and our model for the shift of the electronic levels vs pressure.

and 1.9 eV (652.5 nm) and the relative variation of the ordinary refractive index perpendicular to the c axis deduced from our compressibility measurements. The slope at room pressure, $d\ln(n)/dp$, is clearly positive, in contrast with the original determination of Panfilov *et al.*[11] It is $(1.5\pm0.1)\times10^{-2}$ GPa^{-1}, in agreement with the more recent measurement of Kuroda *et al.*[8] (1.7×10^{-2} GPa^{-1}). The fact that the relative variation of n with pressure is the same for different wavelengths simply shows that the index dispersion does not vary significantly with pressure.

To reproduce the variation of the refractive index versus pressure, we used a one-electron scheme, where the refractive index $n(E,P)$ is given by

$$n^2-1=\frac{A}{V(P)[E_1^2(P)-E^2]}\ , \tag{9}$$

where A is a constant depending on the effective number of electrons participating in transition E_1, and $V(P)$ is the volume of the unit cell.

Here only one energy level, E_1, is used to describe the contribution of all high-energy transitions: In the E⊥c geometry the fundamental transition E_g is nearly forbidden; thus the contribution of the optical gap to the refractive index is negligible.[23,24] We have adjusted the zero-pressure parameters [A and $E_1(0)$] on the very precise determination of Le Toullec *et al.*[23,24] and we get $A=14\,500$ Å^3 eV^2, $E_1=4.842$ eV, with $V=a^2c\sqrt{3}/2$ in Å^3 ($a=3.74$ Å, $c=7.955$ Å). The E_1 value at room pressure fits uv measurements, which show a strong peak at 5 eV and a weaker one near 3.8 eV.[44,45]

The pressure and energy dependences of the refractive index are then given by the variation of the volume of the unit cell and by the shift of E_1. It should be noted that the pressure dependence of the refractive index cannot be explained only by the intrinsic volume dependence. We found it necessary to give a positive shift to E_1: $\Delta E_1/\Delta P\approx10^{-2}$ eV/GPa. Using Eq. (9), the pressure dependence of E_1 (right-hand side of Fig. 4) has been calculated in order to fit experimental $n(E,P)$ values (Fig. 3 and left-hand side of Fig. 4). We have adjusted the variation of E_1 versus pressure (solid line in Fig. 4) using Eq. (10), which separates the intra- and interlayer contributions to the shift of the energy levels,

$$E_1(P)=E_1(0)+\left[\frac{dE_1}{dc_\ell}\right]\Delta c_\ell-\left[\frac{dE_1}{dc_i}\right]\Delta c_i\ , \tag{10}$$

with

$$\frac{dE_1}{dc_\ell}=-0.79\ \text{eV/Å}$$

and

$$\frac{dE_1}{dc_i}=-0.10\ \text{eV/Å}\ .$$

This model, which was initially built to reproduce the pressure dependence of both direct and indirect energy gaps (Sec. IV C), has been successfully applied to E_1 and allows us to calculate the refractive index via Eq. (9), in complete agreement with experimental data. This shows the adequacy of this model for layer compounds. The low value of the interlayer deformation potential (dE_1/dc_i) compared to the intralayer one (dE_1/dc_ℓ) is due to the difference in magnitude of intra- and interlayer interactions.

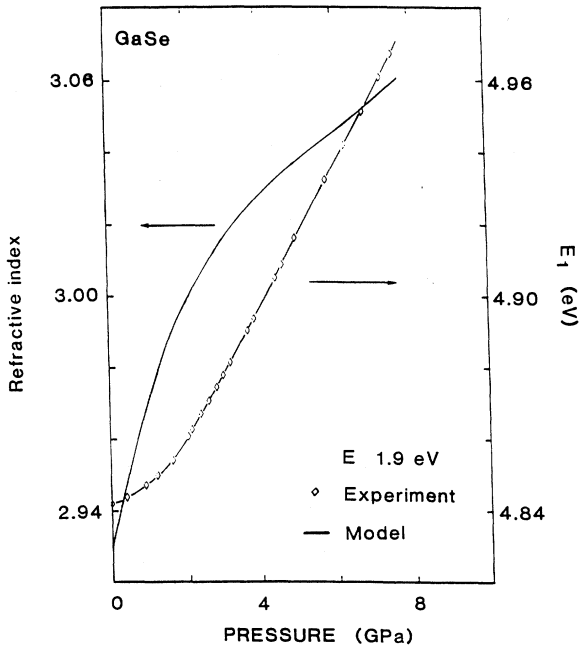

FIG. 4. Variation of the refractive index at 1.9 eV vs pressure (left-hand scale). The experimental data for the value of the uv E_1 level (right-hand scale) is obtained using the one-electron scheme. These data are fitted (solid line) by the model used to explain the shift vs pressure of all electronic levels (see Sec. IV). Only two parameters suffice to account for the $n(E)$ dependence at all pressures.

2. *Absorption coefficient*

Excitonic processes in the absorption edge have been analyzed theoretically by Elliott,[46] who showed how hydrogenoid features appear in the absorption spectrum, and by Toyozawa,[47] who has taken into account the exciton-phonon interaction to explain the line shape of the exciton peaks. Experimentally, at room pressure and low temperature this model has been successfully tested on GaSe by Le Toullec *et al.*:[48] GaSe is a direct-gap material at zero pressure; the possible occurrence[10–14,49,50] of an indirect gap close to the direct gap can be neglected at low temperatures and in a small energy range. The transition is weakly allowed and the exciton exhibits an anisotropic but three-dimensional behavior.

Our results are shown in Figs. 5(a) and 5(b). The solid lines are calculated values and will be explained in the last section. Our measurements cover a larger pressure and photon-energy range than previously published spectra,[10–15,29,51] but in the regions in which a comparison is possible, no significant difference exists with previous re-

ports. The exciton peak can be clearly seen at room pressure. It broadens and disappears between 0.5 and 1 GPa.[10,11,15,29] The absorption edge first shifts towards low energies, up to about 1.3 GPa, and then shifts towards high energies.[14,15] This can be compared to the behavior of InSe, where this reversal occurs around 0.5 GPa.[15] From the shape of the absorption curves, no dramatic change can be seen up to 2 GPa. Above 3 GPa, a low-energy and low-absorption tail appears. The shape of the absorption edge becomes smoother. GaSe behaves like an indirect-gap material, as suggested by earlier experiments[10,14,52] and band-structure calculations.[53] Thus, at high pressure, the absorption coefficient of GaSe can be decomposed into three contributions: (i) the low-energy and low-absorption tail where indirect-absorption processes take place, (ii) the sharp edge at higher energy, which is the range of direct-absorption processes, and (iii) the high-energy edge above both direct and indirect gaps, which has never been quantitatively interpreted, up to now, and which we will assign to the nonparabolic direct continuum.

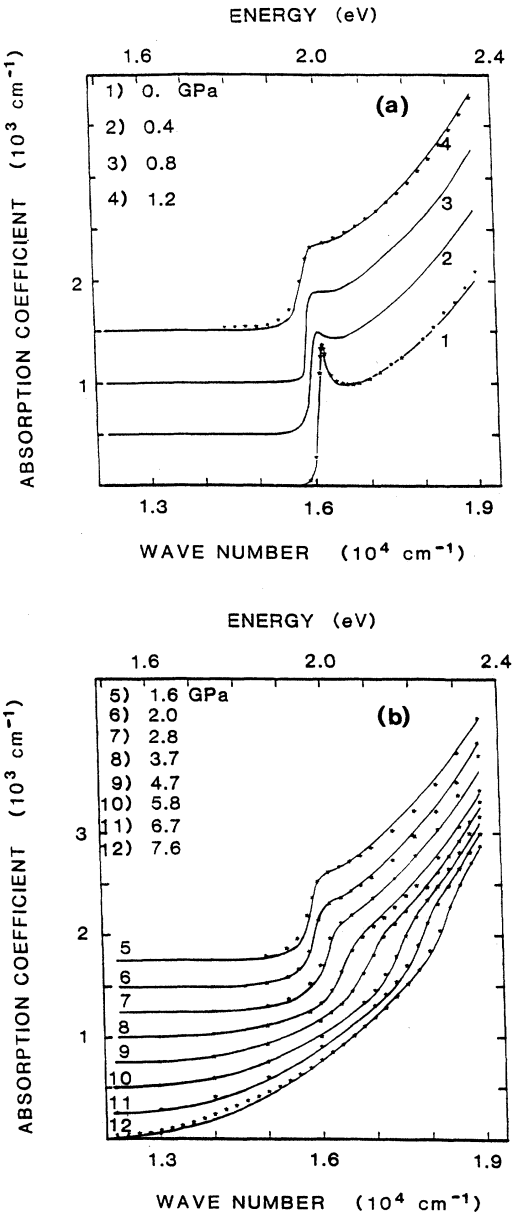

FIG. 5. (a) Absorption coefficient of GaSe in the E⊥c geometry for pressures from 0 to 1.2 GPa. The stars denote experimental values. Solid lines are calculated using the extended Elliott-Toyozawa model (see text). Curves 2–4 are successively shifted up by 500 cm^{-1} on the ordinate axis, with respect to 1, for clarity. (b) Absorption coefficient of GaSe in the E⊥c geometry for pressure from 1.6 to 7.6 GPa. The stars denote experimental values. The solid lines are calculated using the extended Elliott-Toyozawa model (see text). Curves 11–5 are shifted up in ordinates successively by 250 cm^{-1}.

C. Raman scattering

1. Results

The symmetry assignments of the vibrational modes of GaSe are well known.[54,55] The pressure dependence and the Grüneisen parameters for all the modes have been measured up to 1 GPa since 1975,[6,7] and recently up to 3.5 GPa.[8] We have nevertheless done careful Raman-scattering measurements to find out whether a phase transition takes place in the pressure range investigated and to determine the variation of the dynamic effective charge $e_{\perp}^{*}$ versus pressure.

The pressure dependence of Raman-active modes is shown in Fig. 6, (a)–(f) for ε-GaSe and (g)–(j) for γ-GaSe. The Grüneisen parameters are shown in Table I. No evidence[13] for a phase transformation is observed: The frequency jump even for a weak polytypic transition as in GaS (Refs. 30 and 31) is a few cm^{-1}, as compared to the dispersion of our data, which is less than 1 cm^{-1}. Moreover, no break in the slope of any mode appears versus pressure, as observed by Kuroda *et al.*[8] Only the width of the $A_1'^{(2)}$ mode (133 cm^{-1} at room pressure) exhibits a special behavior (Fig. 7), with two maxima, one close to room pressure and the other around 3.2 GPa. Using the two-phonon density of states calculated by Jandl,[42] this effect can be assigned to resonant crossing with two-phonon modes,[56,57] as in GaS.[20] Careful investigation actually has allowed us to observe one of these modes in the spectra. The dashed line in Figs. 6(c) and 6(h) shows the variation of one of these combination modes versus pressure.

2. Analysis

The singular character of the pressure coefficient of intralayer shear modes (the $E''^{(2)}$ mode at 60 cm^{-1} in GaSe) has already been noted.[58] The very small pressure coefficient for this mode can be interpreted as being due to compensation between the decrease in the Ga—Ga bond length, which tends to increase the frequency under pressure, and charge delocalization, which tends to depopulate the Ga_2 radical environment and therefore decrease the Ga—Ga bond strength. This effect is the analogue of what happens in diatomic molecules under pressure (I_2, H_2, etc.), where charge transfer occurs be-

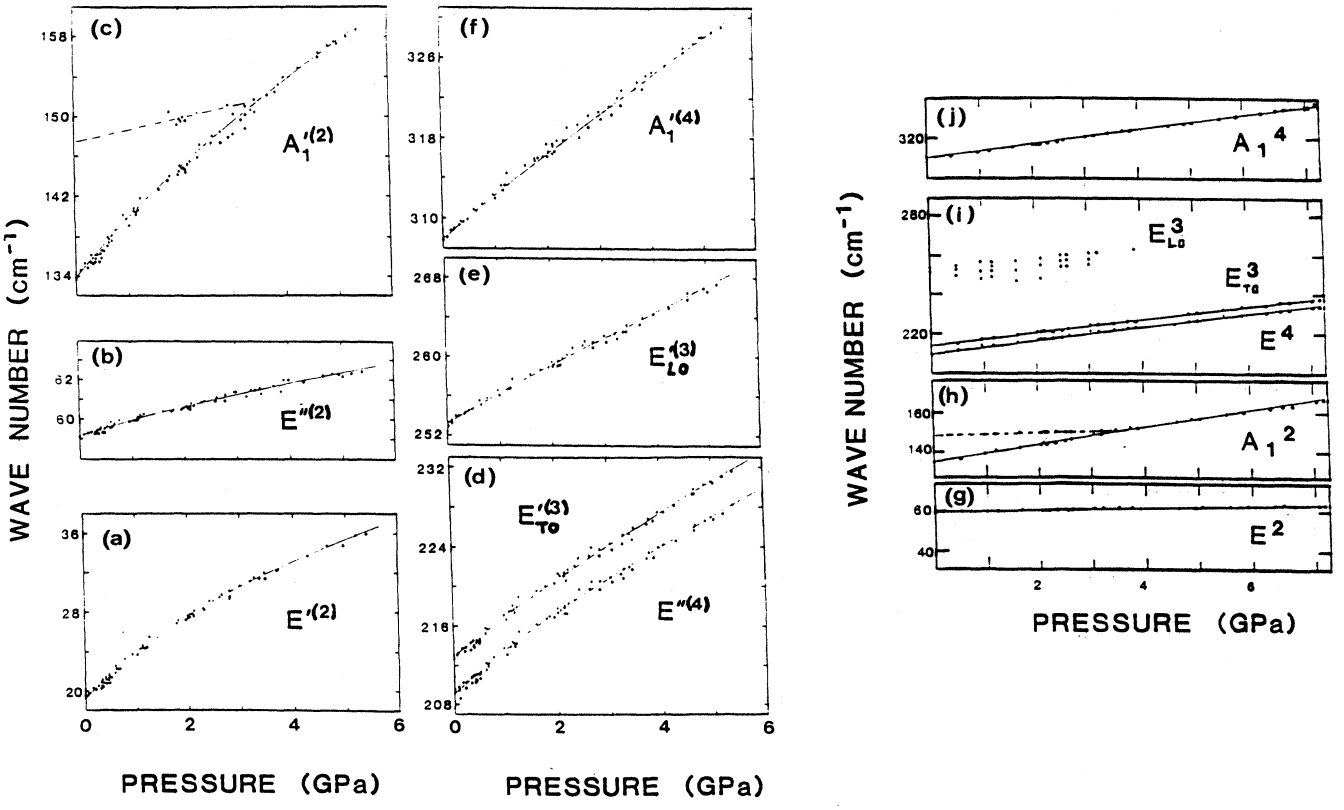

FIG. 6. (a)–(f) Raman scattering on ε-GaSe vs pressure. No evidence for a phase transformation can be seen. The dashed line ($\omega \approx 147$ cm^{-1} at $P=0$ GPa) is a double-phonon mode, which is responsible for the broadening of the $A_1'^{(2)}$ mode around 3 GPa. (g)–(j) Raman scattering on γ-GaSe vs pressure. Same as (a)–(f) otherwise. For symmetry reasons, the low-frequency interlayer shear mode ($E'^{(2)}$ for ε-GaSe) is forbidden in γ-GaSe.

tween the intramolecular space towards the intermolecular region, eventually leading to symmetrization of the bonds when intra- and intermolecular bonds have the same intensity. Here, the two-dimensional GaSe hexagonal sheets which form a GaSe-GaSe layer (Fig. 2) are bonded, within the layer, mostly by Ga—Ga bonds, with a lesser contribution from the intralayer Ga—Se bonds.[31,40–43] Thus, under pressure, charge transfer occurs from the Ga—Ga intramolecular bonds towards the intermolecular (interlayer) space. Obviously, this pressure-induced charge transfer, which gradually increases the interlayer electronic population, should give rise to nonlinear terms in the pressure dependence of the interlayer bulk modulus, which is a gauge of interlayer interactions: This is precisely what was noted in the discussion of the B_{0i}'' parameter in Eq. (6). The large value we have to assign to it, in order to fit the pressure dependence of c, simply represents the increase of the electronic population in the interlayer space. In other words, the charge density between the layers increases at least quadratically with pressure, because of the decrease of interlayer space (B_{0i}') and also because of the total effective number of electrons squeezed out of the intralayer space (B_{0i}''). This will decrease the transverse (intralayer)

TABLE I. Symmetry, frequency, and Grüneisen parameter of the Raman-active modes of ε-GaSe. γ is $(1/\omega)(d\omega/dp)$ and the Grüneisen parameter $\Gamma=\gamma/\chi$ is obtained with $\chi=\chi_{\parallel}+2\chi_{\perp}=37.7\times10^{-3}$ GPa^{-1}.

Modes	$A_1'^{(4)}$	$A_1'^{(2)}$	$E_{LO}'^{(3)}$	$E_{TO}'^{(3)}$	$E''^{(4)}$	$E''^{(2)}$	$E'^{(2)}$
$\omega(p=0)$ (cm^{-1})	307.8	133.8	253.2	212.8	209.3	59.1	19.3
γ (10^{-3} GPa)	15.2±0.6	43.4±1.5	12.6±0.6	20.0±0.0	21.0±1.0	14.2±0.6	245±10
(a)	13	41	11	19		12	200
(b)	14	43	12		21	17	232
Γ	0.40±0.02	1.15±0.04	0.33_5±0.02	0.53±0.03	0.56±0.03	0.38±0.02	6.5±0.3

[a] R. Le Toullec, J. C. Chervin, N. Piccioli, and A. Chevy, Appl. Opt. **20**, 2566 (1981).
[b] Reference 7.

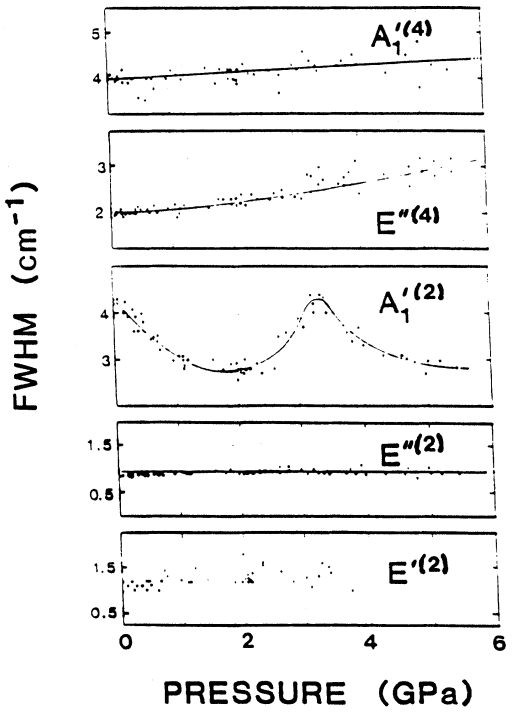

FIG. 7. Variation of the full width at half maximum for the most intense modes of ε-GaSe under pressure. The anomalous behavior of the $A_1'^{(2)}$ mode is due to the crossing with a two-phonon density of states.

effective charge ($e_\perp^*$) and, as we shall see at the end of this paper, increase the longitudinal $e_\parallel^*$ component of the effective charge tensor, which is the main beneficiary of the charge transfer from the Ga—Ga bond. To calculate the transverse effective charge, we have the two relations[59]

$$\epsilon_{0\perp}=\epsilon_{\infty\perp}+\frac{4\pi N}{M}(e_\perp^*)^2\frac{1}{(\omega_{\mathrm{TO}\perp})^2}\ , \tag{11}$$

$$\frac{\epsilon_{0\perp}}{\epsilon_{\infty\perp}}=\left[\frac{\omega_{\mathrm{LO}\perp}}{\omega_{\mathrm{TO}\perp}}\right]^2\ , \tag{12}$$

where $\epsilon_{0\perp}$ is the perpendicular static dielectric constant, $N=k/V(P)$ with k is the number of GaSe dipoles per volume V ($k=2$ and $V=a^2c\sqrt{3}/2$ for γ-GaSe), and M is the reduced mass of the dipole; $\omega_{\mathrm{LO}\perp}$ and $\omega_{\mathrm{TO}\perp}$ are the $E'^{(3)}$ modes. Combining Eqs. (11) and (12), explicitly writing the volume dependence, and substituting $\epsilon_{\infty\perp}=n^2$, where n is the midinfrared value of the refractive index perpendicular to the c axis, we obtain

$$e_\perp^*(P)=e_\perp^*(0)\left[\frac{n^2(P)}{n^2(0)}\frac{V(P)}{V(0)}\frac{\omega_{\mathrm{LO}\perp}^2(P)-\omega_{\mathrm{TO}\perp}^2(P)}{\omega_{\mathrm{LO}\perp}^2(0)-\omega_{\mathrm{TO}\perp}^2(0)}\right]\ , \tag{13}$$

with $e_\perp^*(0)=2.26|e|$.

Using this value, the Szigetti effective charge e^s, which is the real microscopic charge attached to the dipole, is found to be $0.71_5|e|$, with

$$e^s=\frac{3}{\epsilon_\infty+2}e^*\ .$$

This value is smaller than those obtained on ionic compounds[59,60] ($\approx 0.8|e|$), but larger than values obtained in analogous III-V compounds, e.g., $0.57|e|$ for GaP or $0.52|e|$ for GaAs. It confirms the ionicovalent character of intralayer bonds in GaSe.

Figure 8 shows the expected decrease of the perpendicular component of the effective charge versus pressure. The result is in good agreement with the previous value obtained by Kuroda,[8] where the volume dependence was only approximated through the equation of state of InSe (See Fig. 1). To compare GaSe to other compounds, the pertinent value is the Grüneisen parameter[60,61] γ_{e^*} defined by

$$\gamma_{e^*}=-\frac{\partial\ln(e_\perp^*)}{\partial\ln(V)}\ . \tag{14}$$

Our results give a value for $\gamma_{e^*}\approx -0.35$, which compares with values obtained for III-V, II-VI, or group-IV semiconductors.[60,61] This is due again to the fact that perpendicular to the c axis the bonds in layer compounds are ionicovalent and completely analogous to those of classical three dimensionally bonded crystals.

The variation of the static dielectric constant $\epsilon_{0\perp}$ plotted in Fig. 8 is obtained from Eq. (12). The unusual positive sign of the slope observed at low pressure is only due to the high compressibility of GaSe.

IV. DISCUSSION

A. Introduction

Experiments and band-structure calculations indicate that direct and indirect gaps are very close in energy at

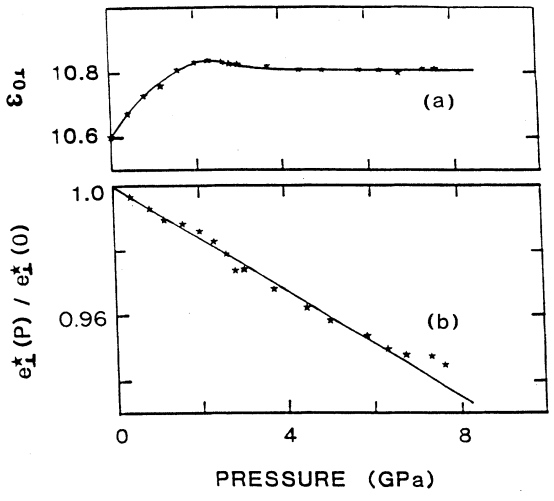

FIG. 8. (a) Variation of the static dielectric constant perpendicular to the c axis, $\epsilon_{0\perp}$, vs pressure, and (b) the related variation of the effective charge $e_\perp^*$. Data denoted by stars are computed from refractive-index and Raman-scattering measurements through the Lyddane-Sachs-Teller relation.

room pressure and temperature. The main problem is then to take into account the two contributions in the absorption process. Moreover, we want to calculate the absorption coefficient well above the direct and indirect gaps. In this section we show first why we can simply add the direct and indirect contributions to the absorption process and then how we take into account the nonparabolic shape of the energy bands. The variation of both direct and indirect gaps will be described with a simple model starting from the known band structure at zero pressure. The results will then be injected into the Elliott-Toyozawa model and a classical indirect-gap absorption law to calculate the total absorption curves. It should be noted that most of the parameters of the Elliott-Toyozawa model will be calculated from the basic physical properties of GaSe because a fitting procedure, although entirely feasible, would not be convincing because of the large number of free parameters. Finally, calculated and experimental absorption curves will be compared and shown to fit within experimental error.

B. Mixing of direct and indirect transitions

1. Indirect transitions

In the region above the indirect excitonic processes ($\alpha > 100$ cm^{-1}), the quadratic behavior for indirect absorption curves has been shown to be correct in GaP or AlAs, for example.[62,63]

In the direct-gap region, enhancement of the indirect processes occurs due to the vicinity of the intermediate states that dominate the transition probability. This enhancement is large when the direct transition is allowed.[62] Understandably, this enhancement would not occur if the direct transition were totally forbidden. This is almost the case here since the direct E⊥c transition is only very weakly allowed in GaSe: The oscillator strength associated with this transition has been shown to be weaker by nearly 2 orders of magnitude than in three-dimensional semiconductors, or in the E∥c polarization.[48] For this reason, we will neglect the enhancement of the indirect absorption coefficient at the energy of the direct gap, which will be a second-order effect, and we use the quadratic dependence throughout, up to the nonparabolic region. Moreover, both contributions (direct and indirect) yield very small ($\alpha < 10^4$ cm^{-1}) absorption coefficients and thus negligible contributions to the real part of the dielectric function, so that we can take the absorption coefficient as additive:

$$\alpha = \alpha_d + \alpha_i \ , \tag{15}$$

where α_d is the contribution of the direct absorption process and α_i the indirect one.

2. Nonparabolic band scheme

Above the energy gaps, we can no longer use a parabolic band scheme, which is only valid close to the gap energy. In all cases in which a precise analysis of $\alpha(h\nu)$ for GaSe has been done, a misfit occurs between calculated and experimental values, about 50 meV above the gap[15,48] or even less. In InSe, *ad hoc* "high-energy–tail" contributions to the absorption coefficient have been cut off exactly at the energy gap[64] for both E_0 and E_1 gaps, but little physical significance can be assigned to this procedure. A deviation from an ideal parabolic band scheme should be a more realistic explanation. The nonparabolicity of the energy bands can be taken into account by introducing the energy dependence of the reduced mass. The simplest way is then to write

$$E(k) = \frac{\hbar^2 k^2}{2m^*(k)} \ , \tag{16}$$

with

$$m^*(k) = m_0^* \left[1 + B \frac{\hbar^2 k^2}{2m_0^*} \right] \ , \tag{17}$$

where m_0^* is the reduced effective mass at $k=0$. Equations (16) and (17) lead to

$$B = \frac{1}{\Delta E_j} \left[1 - \frac{2m_0^*}{\hbar^2 k_j^2} \Delta E_j \right] \ , \tag{18}$$

where ΔE_j is the energy difference between the extrema (maximum and minimum) of the band separated by the wave vector k_j in the j direction. The band structure of GaSe is known in both the $\Gamma \rightarrow M$ and $\Gamma \rightarrow K$ directions. We can then calculate the nonparabolicity coefficient B in these directions. We have found $\Delta E_{\Gamma K} \approx 1.4$ eV with $k_{\Gamma K} \approx 0.25$ and $\Delta E_{\Gamma M} \approx 1.2$ eV with $k_{\Gamma M} \approx 0.21$ in the conduction band. The reduced mass m_0^* is about 0.1 for GaSe,[48–50] which leads to $B \approx 0.56$ eV^{-1} in both directions.

To calculate the absorption coefficient for the direct gap, the classical integration over the density of states transforms to

$$\alpha_d = \frac{1}{E} \int k^2 \delta(\hbar^2 k^2 / 2m^*(k) - (E - E_g^d)) dk \ , \tag{19}$$

where E_g^d is the energy of the direct gap. After integration, we obtain

$$\alpha_d = \frac{1}{2} \left[\frac{2m_0^*}{\hbar^2} \right]^{3/2} \frac{1}{E} \frac{(E - E_g^d)^{1/2}}{[1 - B(E - E_g^d)]^{5/2}} \ ,$$

i.e.,

$$\alpha_d = \alpha_c^d [1 - B(E - E_g^d)]^{-5/2} \ , \tag{20}$$

where α_c^d is the classical law for the direct absorption process.

Before proceeding to apply this model to GaSe under pressure, we verified that it does indeed exactly reproduce well, above the direct gap, the $\alpha(h\nu)$ behavior not only of GaSe at ambient pressure, but also of InSe, which has analogous band structure, without introducing[64] *ad hoc* cutoffs of the high-energy transition tails.

For the indirect absorption process, the classical quadratic law for parabolic bands is

$$\alpha_c^i = \frac{A_i}{E}\{n_\omega[E-(E_g^i-\hbar\omega)]^2 + (n_\omega+1)[E-(E_g^i+\hbar\omega)]^2\} , \quad (21)$$

with

$$n_\omega = n_q \frac{1}{e^{\hbar\omega/kT}-1} ,$$

where E_g^i is the energy of the indirect gap, $\hbar\omega$ the phonon energy of wave vector q, n_q the corresponding density of states, and A_i depends on m_v and m_c, the reduced masses of the valence and conduction bands. It would be rather difficult to transform this equation to take into account exactly nonparabolic terms. For simplicity, we take the same nonparabolicity coefficient at the M and Γ points of the Brillouin zone and introduce the dependence of the effective mass [Eq. (17)] in the classical square law [Eq. (21)] as

$$\alpha_i \approx \alpha_c^i[1+B(E-E_g^i)]^{3/2} . \quad (22)$$

In GaSe the most important phonon involved in the indirect process has been shown to be the $A_1'^{(2)}$ mode (133 cm^{-1} at $P=0$).[65] With this phonon only, the constant A_i has been fitted at high pressure, where the indirect absorption process is well separated from the direct one and found to be $A_i \approx 0.196$.

3. *Elliott-Toyozawa model and final expression of the absorption coefficient*

According to Elliott,[46] electron-hole interaction gives rise to a discrete hydrogenoid series below the gap energy and increases the absorption coefficient in the continuum above the gap. This electron-hole pair (the exciton) interacts with the lattice vibrations of the crystal. Toyozawa[47] has shown that the exciton-phonon coupling leads to a broadening of the exciton lines, which transforms to an asymmetric Lorentzian line shape. In this model the absorption coefficient is

$$\alpha_c^d = A_d|\langle|M|\rangle|^2\frac{(Rm^{*3})^{1/2}}{nE}\left[\sum_i \frac{2R}{i^3}\frac{\Gamma_i/2+b(E-E_i)}{(\Gamma_i/2)^2+(E-E_i)^2} + \int_{E_g}^{\infty}\frac{\Gamma_c/2}{\left[\frac{\Gamma_c}{2}\right]^2+(X-E)^2}\frac{dX}{\left\{1-\exp\left[-2\pi\left[\frac{R}{X-E_g}\right]^{1/2}\right]\right\}^{1/2}}\right] , \quad (23)$$

where A_d is a numerical constant, $\langle|M|\rangle$ the matrix element between the final and initial states, R the effective Rydberg of the exciton $R = R_\infty m^*/\epsilon_0^2$, R_∞ the Rydberg of the hydrogen atom (109 737.3 cm^{-1}), n the refractive index, E_i the ith line of the exciton of width Γ_i ($E_i = E_g - R/i^2$), b the asymmetry parameter of the lines, and Γ_c the width of the continuum.

Using the $\mathbf{k}\cdot\mathbf{p}$ model the variation of the effective mass m^* with pressure is proportional to the gap variation. At low temperature, where interactions with phonons are weak, the exciton width in GaSe is due to crystal defects and has been found[48,66] to be smaller than 4 cm^{-1}. At room temperature this can be neglected with respect to the phonon-induced broadening. The contribution to the width of the exciton peak has been recently calculated for each phonon in GaSe.[66] Their dependence versus pressure can be described as

$$\Gamma_{LO} = k_{LO}\frac{\omega_{LO}^{5/2}}{R^2}n_{LO} \quad (24)$$

for the polar phonon with $k_{LO} \approx 1$, and

$$\Gamma_h = k_h\varepsilon^2\frac{V(P)}{\omega_h^{1/2}}n_h \quad (25)$$

for the homopolar phonon with $k_h \approx 0.1$. The k_{LO} and k_h parameters are considered to be pressure independent and their values are estimated from the results of Piccioli[66] and a deformation potential[49] $\varepsilon \approx 5.5$ eV/Å.

The contribution of the acoustic phonon to the width is neglected. At room pressure and room temperature this contribution is only 0.4 cm^{-1}.

Another process involved in the total width of the excitonic peak has to be taken into account: the interaction between the indirect continuum and the excitonic states.[10] Because of the different pressure coefficient of the direct and indirect gaps, the interaction (broadening) of the exciton by the indirect continuum increases with pressure. So this contribution to the total width of the exciton is expected to increase with pressure. Thus the total width Γ_i [Eq. (23)] of the process will be

$$\Gamma_i = \Omega_i + \Gamma_{LO} + \Gamma_h .$$

$\Gamma_{LO}+\Gamma_h$, the LO- and homopolar-phonon broadening, are taken to be the same for all excitonic levels i. The overlap contribution Ω_i is calculated for each excitonic level along the scheme of Fig. 9.

We shall now proceed to calculate the broadening of the exciton peak Ω_i due to the interaction with the indirect continuum.

In Fig. 9 we define the notations used to calculate Ω_i versus pressure. The phonon involved in the Γ-M transition is obviously the same $A_1'^{(2)}$ mode as for the indirect process. The transition probability is proportional to the density of states n_h of this phonon and to the number of initial and final states. We have

$$\Omega_i \approx n_h \int_0^R N_\Gamma(x) N_M(x) dx \ , \tag{26}$$

with

$$N_\Gamma(x) \approx m_\Gamma^* \sqrt{x} \ ,$$

$$N_M(x) \approx m_M^* (E_g^d - E_g^i - R - \hbar\omega + x)^{1/2} \ ,$$

as shown in Fig. 9.

The nonparabolicity should be taken into account for the conduction band at the M point of the Brillouin zone because of the large energy difference between E_g^i and E_g^d at high pressure. Finally, we find

$$\Omega_i = k_i n_h [1+B(\Delta E')]^{3/2} \frac{1}{2} \left[\frac{2R+\Delta E'}{2} [R(R+\Delta E')]^{1/2} - \left[\frac{\Delta E'}{2} \right]^2 \ln \left[1+2 \frac{R+[R(R+\Delta E')]^{1/2}}{\Delta E'} \right] \right] , \tag{27}$$

with $\Delta E' = (E_g^d - R) - E_g^i - \hbar\omega$. We have used this formula for all the excitonic levels by substituting $E_g^d - R$, with E_i the energy of the ith level. The k_i constant ($k_i \approx 6.5 \times 10^{-3}$ cm) has been adjusted to fit the experimental absorption curves (Fig. 5) over the entire pressure range studied. The shape of the curves below 2 GPa is very sensitive to k_i. These were used to fit parameter k_i independently of the Rydberg exciton and matrix element, which are discussed later.

The final result is shown in Fig. 10. Our calculated values are smaller than the values obtained by Kuroda *et al.*[15] by fitting the direct absorption edge only with the constant Rydberg hypothesis. This hypothesis leads to an overestimate of Γ_1, as can be seen in Eq. (23) if the Rydberg decreases with pressure. We shall see in Sec. IV that the Rydberg decrease is about 40% up to 5 GPa. Nevertheless, both results exhibit the same behavior versus pressure, showing that the model used to calculate the total width of the exciton is adequate.

The asymmetry parameter of the line, b, has been taken to be proportional to Γ_c ($b = k\Gamma_c$, with $k = 18.5 \times 10^{-4}$ cm) in order to reproduce low-temperature data.[48]

The final expression of the absorption coefficient is obtained using Eqs. (15) and (20)–(23) with the model described above to calculate the width Γ_i in Eq. (23). In this calculation of Ω_i, only the decay of the exciton into an M-electron and Γ-hole pair with emission of a phonon was taken into account. The phonon absorption process could also have been included. This was not done here for simplicity because the latter process is not the dominant one: Even at finite temperatures, in indirect absorption processes, the phonon emission process, at energies well above the indirect gap dominates over the ab-

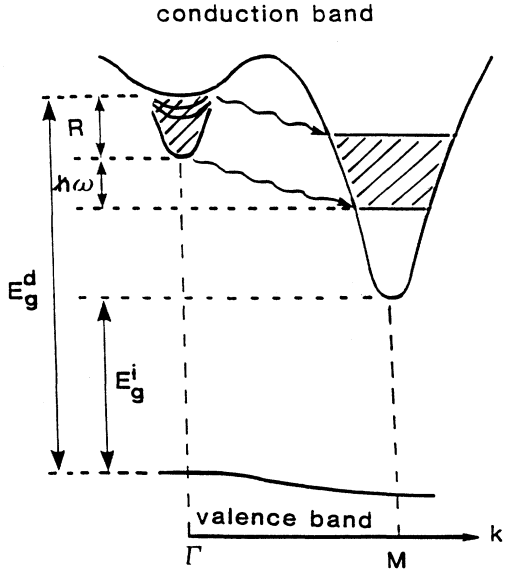

FIG. 9. Destruction of the exciton via the minimum of the conduction band at the M point of the Brillouin zone. The direct exciton of binding energy R is disintegrated by a phonon of energy $\hbar\omega$ and wave vector $k_{\Gamma M}$. E_g^d and E_g^i are, respectively, the direct and indirect energy gaps. The hatched areas represent the initial (at the Γ point) and final (at the M point) densities of states. We assume that the probability of the transition from Γ to M is proportional to these densities of states.

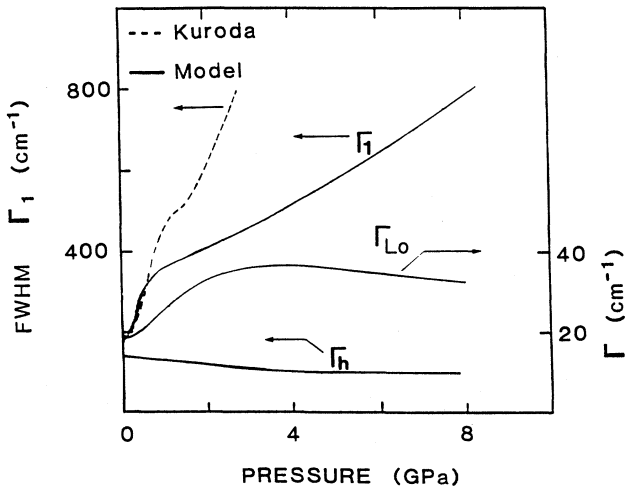

FIG. 10. Variation of the width of the excitonic peak vs pressure. Right-hand side: contribution of the LO phonon. Left-hand side: contribution of the $A_1^{\prime(2)}$ homopolar phonon and total width Γ_1 of the first excitonic level. Γ_1 is calculated with use of the model explained in the text (solid line). The dashed line shows the results obtained by Kuroda *et al.* (Ref. 15) using the constant Rydberg hypothesis, which leads to an overestimation of Γ_1.

sorption process. Moreover, the functional dependence versus energy of both processes is the same, and introduction of phonon absorption processes would simply vary the k_i parameter, which is fitted anyway.

C. Variation of the band gaps versus pressure

The dependence of direct and indirect energy gaps on pressure can be understood by reference to calculated band structures.[49,50]

Construction of the crystal from the isolated atoms allows us to find the origin of the electronic levels and to model their behavior under pressure. Figure 11 summarizes this construction from the left to the right. Shown in column I are the electronic levels of the isolated atoms of Ga and Se. In column II the plane hexagonal lattice of GaSe is built. In column III these planes are deformed: the chair deformation of the layers in the GaSe family. In column IV the intralayer Ga-Ga interaction is switched on, and finally the van der Waals interaction (Se-Se interaction) is introduced (column V). Intralayer interaction (column IV) splits the $4s4p_z$ level into Γ_4 and Γ_1 levels, which would be the gap location of an isolated layer. Thus, this $E(\Gamma_4)$-$E(\Gamma_1)$ splitting depends on the intralayer interaction. The interlayer interaction splits the Γ_1 level into Γ_1^+ and Γ_4^- and the Γ_4 level into Γ_3^+ and Γ_2^-. The gap of the crystal lies between the Γ_4^- and Γ_3^+ levels. Figure 12 shows the electronic levels near the band gap at the Γ and M points of the Brillouin zone and sums up our notations as follows.

$E^{(1)}$ splitting of the $4s$ levels of gallium at the Γ point of the Brillouin zone. $E^{(1)}=E(\Gamma_4)-E(\Gamma_1)$.

$E'^{(1)}$ splitting of the p_{xy} levels of gallium at the M point of the Brillouin zone.

$E_v^{(2)}$ splitting of the p_z levels of selenium in the valence band at the Γ point. $E_v^{(2)}=E(\Gamma_4^-)-E(\Gamma_1^+)$.

$E_c^{(2)}$ splitting of the p_z levels of selenium in the conduction band at the Γ point. $E_c^{(2)}=E(\Gamma_2^-)-E(\Gamma_3^+)$.

$E_c'^{(2)}$ splitting of the p_z levels of gallium in the conduction band at the M point.

Superscripts (1) and (2) refer to energy splittings depending on the intralayer and interlayer forces, respectively (Fig. 11).

The pressure dependences of the direct gap E_g^d and the indirect gap E_g^i are then

$$\frac{dE_g^d}{dP}=\frac{dE^{(1)}}{dP}-\frac{1}{2}\left[\frac{dE_v^{(2)}}{dP}+\frac{dE_c^{(2)}}{dP}\right],$$

$$\frac{dE_g^i}{dP}=-\frac{1}{2}\left[\frac{dE'^{(1)}}{dP}-\frac{dE^{(1)}}{dP}\right]-\frac{1}{2}\left[\frac{dE_v^{(2)}}{dP}+\frac{dE_c'^{(2)}}{dP}\right],$$

and, finally,

$$E_g^d(P)=E_g^d(0)+\frac{dE^{(1)}}{dc_\ell}[c_\ell(P)-c_\ell(0)]-\frac{1}{2}\left[\frac{dE_v^{(2)}}{dc_i}+\frac{dE_c^{(2)}}{dc_i}\right][c_i(P)-c_i(0)], \quad (28)$$

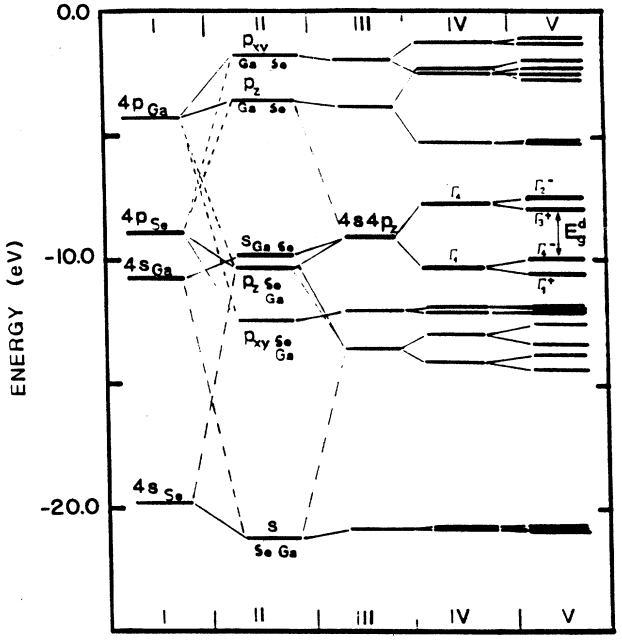

FIG. 11. Construction of the band structure of GaSe from the electronic levels of the isolated atoms [after Schlüter (Ref. 49) and Bourdon (Ref. 50)]. From left to right: we start from the neutral atoms (I) and build hexagonal plane sheets (II); we distort these sheets (III) and build a layer with two sheets (IV); and then we bring the layers close to each other (V) (switching on the interlayer interaction).

$$E_g^i(P)=E_g^i(0)-\frac{1}{2}\left[\frac{dE'^{(1)}}{dc_\ell}-\frac{dE^{(1)}}{dc_\ell}\right][c_\ell(P)-c_\ell(0)]-\frac{1}{2}\left[\frac{dE_v^{(2)}}{dc_i}+\frac{dE_c'^{(2)}}{dc_i}\right][c_i(P)-c_i(0)]. \quad (29)$$

In this model all the quantities dE/dc are negative be-

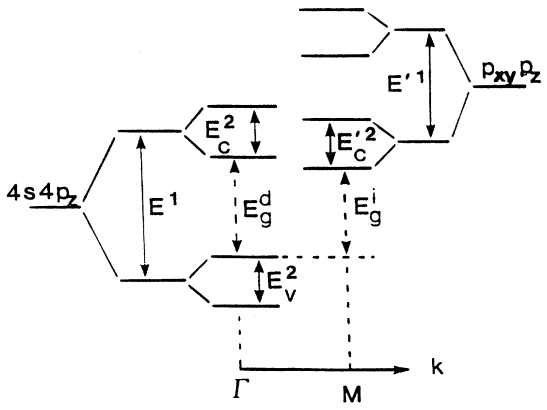

FIG. 12. Simplified band structure of GaSe at the Γ and M points of the Brillouin zone. Notations used are defined in text. According to Fig. 11, superscript (1) indicates that levels are sensitive to intralayer interactions and superscript (2) indicates that levels are sensitive to the interlayer interactions. E_g^d and E_g^i are, respectively, the direct and indirect energy gap.

cause of the increase of the splittings with pressure. For simplicity, we also assume that they are constant. So, according to Eqs. (28) and (29) we only need three deformation potentials, one for the s levels, one for the p_{xy} levels, and one for the p_z levels, to reproduce both the direct- and indirect-gap dependence versus pressure.

D. Discussion of the parameters

1. Deformation potentials

Our experimental results show that the indirect edge of GaSe is clearly observable only for pressures above 3 GPa when it is unambiguously separated from the direct edge. At lower pressures the uncertainties are too large and we have no data points reported in Fig. 13. On the other hand, the direct edge can be followed up to 8 GPa but the uncertainties increase with pressure. Our results are in complete agreement with recent data,[8] as can be seen in Fig. 13. We have adjusted the three deformation potentials by simultaneously fitting the low-pressure behavior of the direct gap and the high-pressure behavior of the indirect gap. This gives an estimate of the energy gaps where no data are available. Then we refined these estimations by fitting the total absorption coefficient.

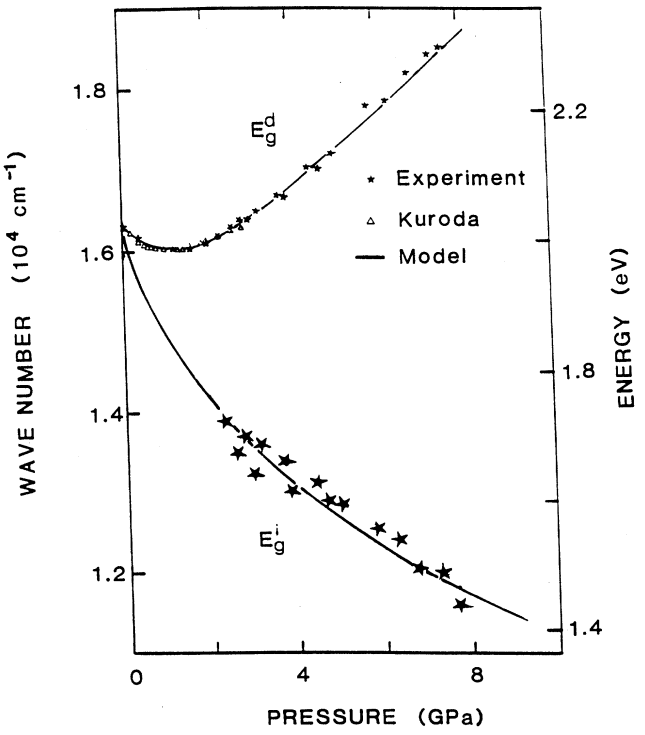

FIG. 13. Variation of the direct and indirect energy gaps vs pressure. Stars denote experimental values obtained from the fit of the absorption coefficient α. Triangles denote the results of Kuroda *et al.* (Ref. 15). Solid lines are calculated with our model, which uses only three deformation potentials: one for the s levels, one for the p_{xy} levels, and one for the p_z levels (see text).

The final values of the three deformation potentials used in the model are

$$\frac{dE^{(1)}}{dc_\ell}=\frac{ds_{\text{Ga—Ga}}}{dc_\ell}=-2.40\pm0.05\ \text{eV/Å}$$

for the Ga—Ga bond,

$$\frac{dE'^{(1)}}{dc_\ell}=\frac{dp_{xy\ \text{Ga}}}{dc_\ell}=-5.3\pm0.2\ \text{eV/Å}$$

for the p_{xy} gallium levels, and

$$\frac{dE_c^{(2)}}{dc_i}=\frac{dE_v^{(2)}}{dc_i}=\frac{dE_c'^{(2)}}{dc_i}=\frac{dp_z}{dc_i}=-0.60\pm0.05\ \text{eV/Å}$$

for both the p_z levels of gallium and selenium.

These results are consistent in that the levels that are most sensitive to pressure correspond to the less localized electrons. The value of the deformation potential of p_{xy} orbitals strongly depends on the approximations made for the p_z level of gallium. For example, if we choose to minimize the contribution of the p_z levels of gallium, i.e., to assume a zero value for this deformation potential ($dE_c'^{(2)}/dc_i=0$), we obtain an upper value of -6 eV/Å for the p_{xy} levels. In all cases the ratio between the p_{xy} (intralayer interaction) and the p_z (interlayer interaction) deformation potentials corresponds to the ratio of covalent to van der Waals forces, in agreement with the model.

At room pressure, direct and indirect gaps have been found to be, respectively, $E_g^d=2.0196\pm0.0005$ eV and $E_g^i=2.010\pm0.030$ eV. If GaSe is an indirect-gap material at ambient pressure, the energy difference between the two gaps is about 10 meV. This confirms previous experimental results and band-structure calculations.

Under high pressure, GaSe becomes an increasingly indirect-gap material due to the increased splitting of the direct and indirect gaps. At zero pressure, we have found for the direct gap

$$\frac{dE_g^d}{dP}=-(4.5\pm1.0)\times10^{-2}\ \text{eV/GPa}\ .$$

This value is the classical result obtained for this gap in both experimental[10–15,51] or theoretical papers.[52]

The pressure coefficient for the indirect gap at atmospheric pressure is

$$\frac{dE_g^i}{dP}=-(15.5\pm2.0)\times10^{-2}\ \text{eV/GPa}\ .$$

This coefficient is stronger than that calculated by Bourdon[52] (-10.5×10^{-2} eV/GPa), the difference coming from a different location of the minimum of the conduction band in this paper. The value found here is consistent with experimental results of Niilisk[10,51] (-13×10^{-2} eV/GPa) and Besson[12] (-11×10^{-2} eV/GPa). The latter result is based on a linear extrapolation between 0 and 0.6 GPa and thus could only give a lower limit for the absolute value of the pressure coefficient.

2. Determination of the pressure variation of R and $\langle |M| \rangle$

At this point we only need two parameters to fit the total absorption coefficient at any pressure: the exciton Rydberg R and the transition probability between valence and conduction band, $\langle |M| \rangle^2$.

The decrease of the direct contribution to the absorption coefficient [Eq. (23) and Fig. 5] can be reproduced either by a decrease of the exciton Rydberg, or of the transition probability $\langle |M| \rangle^2$, or both, but only a significant change of the exciton Rydberg can account for the smoothing out of the absorption curves. The following discussion on the physical processes involved in the change of R and $\langle |M| \rangle$ versus pressure is an attempt to separate out the two contributions.

The exciton Rydberg for an anisotropic material is

$$R = R_\infty \frac{m^*}{(\epsilon_{0\perp}^2 \epsilon_{0\parallel})^{2/3}} , \tag{30}$$

where $\epsilon_{0\parallel}$ is the static dielectric constant parallel to the c axis. The variation of all quantities involved is known, except for $\epsilon_{0\parallel}$. At pressures above 1.5 GPa the $n=1$ exciton level is not distinguishable from the continuum, and thus R cannot be obtained directly from its position relative to the edge. On the contrary, at low pressures (below 1 GPa) the decrease of R (Fig. 14) can be accounted for only by an increase of $\epsilon_{0\parallel}$ versus pressure, which is $d(\epsilon_{0\parallel})/dP \approx (1 \pm 0.5)$ GPa^{-1}. Figure 14 shows the estimated values of R versus pressure. The upper curve, (a), is obtained by taking $\epsilon_{0\parallel}$ constant and equal to its room-pressure value. The lower one, (b), is the other extreme, the isotropic case with $\epsilon_{0\parallel}=\epsilon_{0\perp}$. Clearly, the actual behavior [dashed line (c)] lies between the two and would tend to show an increase of $\epsilon_{0\parallel}$ with pressure. In three-dimensionally bonded crystals, or in the $\epsilon_{0\perp}$ component of GaSe (see Sec. III C 2), one does not observe any such increase. As a matter of fact, due to charge delocalization the dielectric function is usually expected to decrease with pressure in ionic crystals, and it does. Such is not the case apparently for the parallel component of ϵ_0 in layer crystals: ϵ_0 is made of two contributions: one, ϵ_∞ (in the mid-infrared region) comes from all electronic processes, and the other [Eq. (11)] comes from the lattice vibrations. The latter contribution is remarkably small in GaSe for the parallel configuration: $\omega_{\mathrm{TO}\parallel}=236$ cm^{-1} and $\omega_{\mathrm{LO}\parallel}=244$ cm^{-1}, and the microscopic effective charge $e_\parallel^s$ is about half of $e_\perp^s$. This must be related to the layered character of the material: Indeed, for isolated layers (infinite interlayer spacings) there would be no TO-LO splitting. This means that the microscopic effective charge $e_\parallel^s$ is small, since the charge density in the interlayer space is small. Under pressure, charge transfer occurs from the intra- to the interlayer space. This decreases the Ga—Ga bond charge, as we saw before, also somewhat decreases $e_\perp^s$ (effective charge for vibrations within the layer), but, in turn, must increase the interlayer charge density. This distorts the charge configuration around the Se^- ions, effectively increasing the $e_\parallel^s$ component (in the interlayer space). Another way to see this is to note that the Se^- ions are in an effective threefold coordination with Ga atoms in the isolated layer, but tend to a sixfold coordination when layers come close together. This will increase their effective ionicity for vibrations along the c axis. We thus expect the parallel reststrahlen of GaSe to become analogous to the perpendicular component in the region of 5–10 GPa, where bonds are isotropic in magnitude. The other contribution is ϵ_∞. Let us note that the difference between ordinary and extraordinary refractive indices (0.33) is about 1 order of magnitude larger than values observed in anisotropic crystals of the same series (CdS, ZnS, CdSe, etc.), but equal to that of other layered compound (GaS). Clearly, this very-high-index anisotropy is linked to the layer character of GaSe and GaS and must decrease under pressure, as indeed it does in GaS.[22] Using the results obtained on GaS for the variation of the refractive-index anisotropy under pressure and the values we have found for $\epsilon_{\infty\perp}$, we can infer the variation of the parallel component of ϵ_∞. At this point we shall examine two different schemes to calculate the evolution of $\epsilon_{0\parallel}$ with pressure, in order to account for the variation of R.

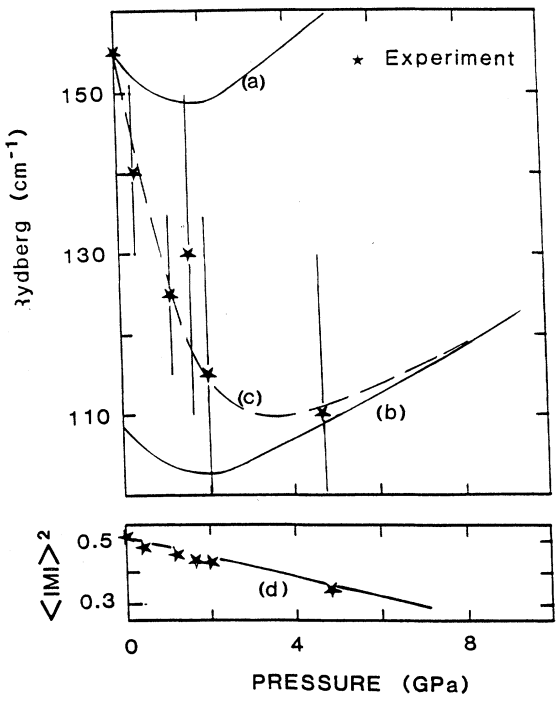

FIG. 14. Variation of the Rydberg (c) and of the matrix element for the direct transition (d) vs pressure. These two parameters (stars) are determined by fitting the total absorption coefficient α with the Elliott-Toyozawa model. For the Rydberg, the upper curve, (a), is the result of calculation using the $\epsilon_{0\parallel}=$const hypothesis; the lower curve, (b), uses the purely isotropic hypothesis; the dashed line, (c), is obtained by using a continuous variation of ϵ_0. The only parameter is $\epsilon_{0\parallel}$, and we assume that it increases with pressure (see text). The lower part of the figure shows the decrease of the probability of the direct transition. In fact, this transition is allowed by accidental hybridization at $P=0$ GPa between s and p levels.

(a) In this first hypothesis, we simply assume that the observed decrease of the perpendicular effective charge is compensated by an equal increase of the parallel component ("charge-transfer" mechanism).

(b) A more drastic evolution can be envisaged by assuming that around 5 GPa, where GaSe behaves as a *macroscopically* isotropic medium for a number of properties (compressibility, interatomic restoring forces), ϵ_0 also tends to be isotropic.

With hypothesis (a) of a total charge transfer occurring between the perpendicular and the parallel effective charges, i.e., $\Delta e^s=0$, we calculate, using the Raman-scattering results, the microscopic effective charge $e_{\parallel}^s(P)$:

$$e_{\parallel}^s(P)=e_{\parallel}^s(0)+[e_{\perp}^s(0)-e_{\perp}^s(P)] .$$

With these two quantities ($\epsilon_{\infty\parallel}$ and $e_{\parallel}^s$) and the volume dependence versus pressure, we can deduce, via Eqs. (11) and (13), $\omega_{\mathrm{LO}}^2-\omega_{\mathrm{TO}}^2$ for the components parallel to the c axis. We take $(\omega_{\mathrm{LO}}+\omega_{\mathrm{TO}})_{\parallel}$ to increase regularly with pressure, to a first approximation, in the same ratio as the perpendicular components. We then get the LO-TO splitting for the parallel components and the static dielectric function $\epsilon_{0\parallel}$. This last hypothesis is not important for the determination of $\epsilon_{0\parallel}$; the relative error can be estimated to be 2%. The results are shown in Fig. 15(a) and in Fig. 15(b), curve 2. The LO-TO splitting is experimental for the direction perpendicular to the c axis and is calculated otherwise.

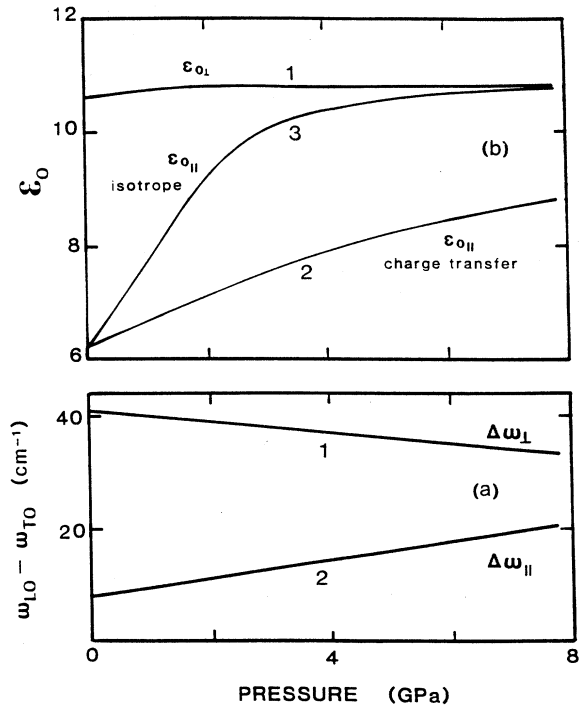

FIG. 15. (a) LO-TO splittings. Curve 1 ($\Delta\omega_{\perp}$) is experimental, while curve 2 ($\Delta\omega_{\parallel}$) is calculated using the charge-transfer hypothesis (see text). (b) Static dielectric constant. Curve 1 ($\epsilon_{0\perp}$) is "experimental"; curves 2 and 3 represent calculated $\epsilon_{0\parallel}$: curve 2 using the charge-transfer hypothesis, and curve 3 is obtained via Eq. (31) and corresponds to a progressive change to an isotropic crystal, analogous to the compressibility behavior.

In case (b), to account for the evolution of both components of $\epsilon_{0\parallel}$ (vibrational and electronic) with a simple expression, we just take the parallel dielectric function to increase regularly with decreasing bond anisotropy, the gauge of which is the compressibility anisotropy. We take the difference in the dielectric function components to be proportional to it:

$$\epsilon_{0\parallel}-\epsilon_{0\perp}=A\left[\frac{\chi_a-\chi_c}{\chi_a}\right] \quad \text{with } A=0.98 . \tag{31}$$

The result in the calculation of R using this functional dependence is shown in Fig. 14. The precise dependence of $\epsilon_{0\parallel}$ on P is by no means crucial to fit the data. Equation (31) causes $\epsilon_{0\parallel}$ to increase from 6.2 to 10.5 at about 5 GPa [Fig. 15(b), curve 3]. The value at 5 GPa may be different by as much as 20% from the latter value without any contradiction of our model. The important point here is that $\epsilon_{0\parallel}$ increases very fast with pressure [$d(\epsilon_{0\parallel})/dP\approx 1$ GPa^{-1} compared to $d(\epsilon_{0\perp})/dP\approx 0.15$] due to charge redistribution from the intra- to the interlayer space. When we use the values of $R(P)$ from Eqs. (30) and (31), we find that in case (b), to fit the absorption coefficient $\alpha(h\nu)$ versus pressure, we have to decrease the probability of the transition between the valence and conduction bands linearly with pressure [Fig. 14(d)]. Between 0 and 5 GPa, $\langle |M| \rangle^2$ decreases by 40% and $\langle |M| \rangle$ by $\approx$20%. The explanation is that the transition that is weakly allowed at atmospheric pressure by accidental hybridization between s and p levels in the valence band becomes less allowed under pressure. This indicates that s and p levels do not have the same deformation potentials and that their hybridization decreases with pressure. This effect is predicted by the model we have used to reproduce the band-gap variation with pressure (see Sec. IV D 1).

With the above expressions for the absorption coefficient, the absorption edge can be fitted, at all pressures investigated in the region 12 000–19 000 cm^{-1} (1.5–2.4 eV), well within experimental errors on the absolute value of α (5%). This is shown in Figs. 5(a) and 5(b) as solid lines. This network of curves is almost entirely calculated from the model we derived from compressibility measurements and the gap variation (Fig. 13). The only fitted parameters are the k_i parameter in Eq. (27), the pressure dependence of the exciton Rydberg, and the matrix element for the transition. Here the dependences of the latter quantities are those shown in Fig. 14, which correspond to curve 3 in Fig. 15(b) for $\epsilon_{0\parallel}$. At low pressure (<1 GPa) the precision of our pressure gauge is insufficient to provide reliable data. Nevertheless, in Fig. 5(a), curves 2 and 3 at 0.4 and 0.8 GPa entirely fit previously[9–15] published results in this pressure range. In this fit we had to assume a large increase of $\epsilon_{0\parallel}$ with pressure in both schemes discussed above. It is possible to check the validity of this assumption, although the static dielectric tensor has not been measured under pressure in any layered crystal. This can be done by comparison with

InSe: In Fig. 1 we note that the $c(P)$ of InSe is analogous to that of GaSe under pressure. As a matter of fact, it is strictly identical if one compares GaSe at 0.8 GPa and InSe at ambient pressure. From this point of view, InSe at ambient pressure behaves like GaSe at 0.8 GPa. This is entirely reflected in the band structure: The direct-gap pressure dependence of both compounds is identical when one shifts GaSe down in pressure by 0.8 GPa. Among other features, the minimum value of $E_g^d(P)$ is at 0.45 GPa for InSe, and around 1.3 GPa for GaSe—that is, some 0.8 GPa higher. InSe thus appears to be a pressurized version of GaSe. This analogy may now be used as a check on our model for the evolution of GaSe regarding its ionicity under pressure—that is, the increase of $\epsilon_{0\parallel}$ under pressure (Fig. 15). Rather than compare the dielectric-constant anisotropy of InSe at ambient pressure and GaSe at 0.8 GPa, it is physically more meaningful to compare the anisotropy of the Szigetti effective charges $A=e_\perp^s/e_\parallel^s$, using Eqs. (11) and (12). We will now proceed to compare this ratio in InSe, and in pressurized (0.8 GPa) GaSe, along the lines of the two schemes [Fig. 15(b), curves 2 and 3] discussed previously.

(i) InSe. The lattice parameters are[67] $a=4.002$ Å and $c=24.946$ Å, which leads to the thickness per layer $\bar{c}=8.315$ Å with two dipoles per unit cell. The dielectric constants[64] and the polar-mode wave numbers[68–70] are, respectively, $\epsilon_{\infty\perp}=7.34$, $\epsilon_{\infty\parallel}=7.0$, $\omega_{\mathrm{LO}\perp}=214$ cm^{-1}, $\omega_{\mathrm{TO}\perp}=178$ cm^{-1}, $\omega_{\mathrm{LO}\parallel}\approx 200$ cm^{-1}, and $\omega_{\mathrm{TO}\parallel}\approx 190$ cm^{-1}. The Szigetti charges are then $e_\perp^s=0.766|e|$ and $e_\parallel^s=0.408|e|$, and the room-pressure charge anisotropy A is 1.88.

(ii) GaSe. In GaSe at ambient pressure, A is 2.07, with $e_\perp^s=0.715|e|$ and $e_\parallel^s=0.346|e|$. The fact that the Szigetti charges of InSe are larger than those of GaSe only indicates that InSe is more ionic than GaSe because the outer electrons of In are less bonded than those of Ga, i.e., the chemical In—In bond is weaker than the Ga—Ga bond. This higher ionicity can be viewed as inducing an inner pressure via the Coulomb interaction,[71] making InSe analogous to compressed GaSe. Under pressure, we can use either the charge-transfer hypothesis [Fig. 15(a) and Fig. 15(b), curve 2] or the "isotropic" scheme [Fig. 15(b), curve 3] and a more rapid increase of the $\mathrm{LO}_\parallel$-$\mathrm{TO}_\parallel$ splitting coherent with this hypothesis. We find in the first case, for GaSe at 0.8 GPa,

$$A=1.92\ ,$$

and, in the second case,

$$A=1.63\ .$$

The actual value is 1.88 for InSe, which is rather close to the first case, the actual pressure dependence probably falling between the two extremes. The significant point here is that this order-of-magnitude comparison also points to a sizable increase of $\epsilon_{0\parallel}$ versus pressure in GaSe.

V. CONCLUSIONS

We have presented experimental results on GaSe under high pressure: measurements of compressibility up to 20 GPa, refractive index, Raman scattering, and absorption coefficient up to 8 GPa. In the experiments there is no evidence for a phase transition. The first conclusion is that the layered structure of GaSe is remarkably stable under pressure.

The decrease of compressibility along the c axis (from 27.4×10^{-3} GPa^{-1} at room pressure to 6.1×10^{-3} GPa^{-1} at 5 GPa) is quantitatively reproduced by a model which separates the intra- and interlayer contributions to the total compressibility, using the isotropic layer model which has been shown to be valid in GaS. This model indicates that above 5 GPa, due to the large variation of the interlayer compressibility, the inter- and intralayer interactions are of the same order of magnitude. From this point of view, GaSe becomes, under pressure, a macroscopically isotropic material. This evolution comes without any reconstruction of the material and without any change in nature of the interactions, although it entirely retains its microscopic two-dimensional structure.

The pressure coefficient of the refractive index is positive: $d\ln(n)/dp=(1.5\pm0.1)\times10^{-2}$ GPa^{-1}. From the refractive-index values and Raman-scattering measurements, we have deduced the pressure dependence of the static dielectric constant $\epsilon_{0\perp}$ perpendicular to the c axis. The parallel components of ω_{LO} and ω_{TO} are Raman inactive, so that $\epsilon_{0\parallel}$ cannot be deduced directly from our results. As expected, this determination shows that, perpendicular to the c axis, GaSe can be considered a classical compound with strong ionicovalent bonds. The unusual positive slope $d\epsilon_{0\perp}/dp$ at low pressure is only due to the large compressibility of GaSe, and the transverse effective charge perpendicular to the c axis decreases as in other classical III-V, II-VI, or group-IV semiconductors. This explains the very small (according to the Zallen model) Grüneisen parameter of the rigid-layer shear mode ($E''^{(2)}$): The decrease of the effective charge is due to charge delocalization that depopulates the Ga—Ga bond and thus softens the force constant under pressure. This effect is partly balanced by the "classical" pressure effect, which tends to decrease the interatomic distances and to increase the frequencies.

The last point in this work is the analysis of the absorption coefficient. We have built a model to explain the pressure shift of the electronic levels based on the band structure of GaSe. This model has been successfully applied for the direct gap, the indirect gap, and near-uv level. It allows us to describe the pressure shift of the absorption curve as well as the refractive index for all (λ,p) points. According to this model, the deformation potentials have been found to be -2.4 eV/Å for the s level of Ga, -5.3 eV/Å for the p_{xy} level of Ga, and -0.6 eV/Å for the p_z levels of Ga and Se. The low value of the latter is due to the large compressibility in the z direction, especially between the layers. The indirect gap at $P\neq0$ can be extrapolated to $P=0$, to show that GaSe is a weakly indirect-gap material at room pressure. The difference between the direct and indirect gap is no more than 10 meV. The absorption curve has been calculated for all pressures using the Elliott-Toyozawa model. Some minor extensions have been done on this model to account for all the data. First, because of the large energy range investigated, band nonparabolicity has been taken into ac-

count to calculate both direct and indirect absorption coefficients, and, secondly, the width of the excitonic peak has been modeled because a fitting procedure would be inadequate for this model, which contains many nonindependent parameters. Thus only one constant and two adjustable pressure-dependent parameters have been used: the transition probability $\langle |M| \rangle^2$ and the static dielectric constant parallel to the c axis, $\epsilon_{0\|}$. With only these parameters, the total absorption curves for all pressures have been calculated. Comparison with experiment shows that it is impossible to keep the transition probability constant versus pressure: it must have decreased by some 40% at 5 GPa. This effect can be related to the decrease of the accidental hybridization occurring at room pressure between s and p levels that do not have the same deformation potentials. The fit with experimental data also imposes an increase of $\epsilon_{0\|}$ under pressure. This reduces the anisotropy of the dielectric-constant tensor by at least a factor of 3, and it may become isotropic above 5 GPa. This could be quantitatively confirmed by ir or capacitance measurements under pressure, which are not available at the present time. In any case, GaSe does evolve, under pressure, to a bonding scheme where the interlayer van der Waals region is as strongly bonded as the ionicovalent layers. In this sense it is macroscopically isotropic although still microscopically two dimensional. It is then in the same structural class as quasi-two-dimensional systems such as perovskites of the K_2NiF_4 family at ambient pressure, or quasi-one-dimensional systems such as the ABX_3 series, e.g., $CsCdBr_3$. In those microscopically low-dimensional systems, ionicovalent planes or chains are separated by planes or chains of ionized alkali-metal ions, the outer electrons of which have a rare-gas configuration (closed shell). In these systems, at room pressure, the Coulomb interaction brings about an equivalent inner pressure[72] of a few GPa that packs the ionicovalent planes or chains and makes the crystal macroscopically three dimensional, in the same way as hydrostatic pressure does in GaSe. When high pressure is applied to these systems, the ionic planes or chains ("van der Waals" regions) must rapidly reach their highly incompressible hard-sphere regime, and the bulk of compression is taken by the ionicovalent regions. This has been shown for one-dimensional systems[72] and must also be true for two-dimensional perovskites. They are then analogous to GaSe or GaS above 10 GPa, where the interlayer space becomes more rigid than the layers themselves (hard-sphere regime for the Se^{2-} ions). A number of interesting properties must exist in relation to this highly nonlinear behavior, such as large charge transfer and variations of the dielectric constant by phonons that displace the ions in the system, which should contribute to new terms to the electron-phonon coupling. Thus the continuous transition, under pressure, of the bonding scheme in layered structures may serve as a model for understanding some aspects of other low-dimensional systems.

ACKNOWLEDGMENTS

Physique des Milieux Condensés is unité associé No. 782 au Centre National de la Recherche Scientifique.

[1]H. Hahn, Angew. Chem. **65**, 238 (1953).
[2]W. Schubert, E. Dorre, and M. Kluge, Z. Metallkd. **46**, 216 (1955).
[3]F. Jellinek and H. Hahn, Z. Naturforsch. **16**, 713 (1961).
[4]J. C. J. R. Terhell and R. M. A. Lieth, Phys. Status Solidi A **5**, 719 (1971).
[5]A. Kuhn, R. Chevalier, and A. Rimsky, Acta Crystallogr. Sect. **31**, 2841 (1975).
[6]R. N. Tyte, W. Richter, and M. Rautenberg, Verh. Dtsch. Phys. Ges. (VI) **10**, 403 (1975).
[7]E. A. Vinogradov, G. N. Zhizhin, N. M. Melnik, S. I. Subbotin, V. V. Panfilov, K. R. Allakhverdiev, S. S. Babaev, and V. F. Zhitar, Fiz. Tverd. Tela (Leningrad) **22**, 792 (1980) [Sov. Phys.—Solid State **22**, 434 (1980)].
[8]N. Kuroda, O. Ueno, and Y. Nishina, Phys. Rev. B **35**, 3860 (1987).
[9]S. I. Subbotin, V. V. Panfilov, L. F. Vereshchagin, R. T. Molchanova, and G. A. Akhundov, Dokl. Akad. Nauk. SSSR **202**, 1039 (1972) [Sov. Phys.—Dokl. **17**, 126 (1972)].
[10]J. M. Besson, K. P. Jain, and A. Kuhn, Phys. Rev. Lett. **32**, 936 (1974).
[11]V. V. Panfilov, S. I. Subbotin, L. F. Vereshchgagin, I. I. Ivanov, and R. T. Molchanova, Phys. Status Solidi B **72**, 823 (1975).
[12]J. M. Besson, Nuovo Cimento **38**, 418 (1977).
[13]S. I. Subbotin, V. V. Panfilov, and R. T. Molchanova, Phys. Status Solidi A **39**, 357 (1977).
[14]M. Gauthier, A. Polian, and J. M. Besson, J. Phys. (Paris) Colloq. **45**, C8-65 (1984).
[15]N. Kuroda, O. Ueno, and Y. Nishina, J. Phys. Soc. Jpn. **55**, 581 (1986).
[16]E. Lendway, A. Kuhn, A. Chevy, and T. Ceva, J. Mater. Sci. **6**, 305 (1971).
[17]G. J. Piermarini and S. Block, Rev. Sci. Instrum. **46**, 973 (1975).
[18]A. Jayaraman, Rev. Mod. Phys. **55**, 65 (1983); **57**, 1013 (1986), and references therein.
[19]J. M. Besson and J. P. Pinceaux, Rev. Sci. Instrum. **50**, 541 (1979).
[20]A. Polian, J. C. Chervin, and J. M. Besson, Phys. Rev. B **22**, 3049 (1980).
[21]H. K. Mao, P. M. Bell, J. W. Shaner, and D. J. Steinberg, J. Appl. Phys. **49**, 3276 (1978).
[22]A. Polian, J. M. Besson, M. Grimsditch, and H. Vogt, Phys. Rev. B **25**, 2767 (1982).
[23]R. Le Toullec, N. Piccioli, M. Mejatty, and M. Balkanski, Nuovo Cimento B **38**, 159 (1977).
[24]N. Piccioli, R. Le Toullec, M. Mejatty, and M. Balkanski, Appl. Opt. **16**, 1236 (1977).
[25]K. Vedam and P. Limsuwan, J. Chem. Phys. **69**, 4762 (1978).
[26]P. W. Bridgman, Proc. Acad. Sci. **49**, 3 (1913); **74**, 399 (1942).
[27]F. D. Murnaghan, Proc. Nat. Acad. Sci. U.S.A. **30**, 244 (1944).,
[28]J. R. MacDonald, Rev. Mod. Phys. **38**, 669 (1966); **41**, 316 (1969).
[29]J. M. Besson, R. Le Toullec, J. P. Pinceaux, A. Chevy, and H. Fair, High Temp.-High Pressures **7**, 710 (1975).
[30]H. Shinriki, K. Takemura, K. Asaumi, and S. Minomura, in

Proceedings of the 8th AIRAPT Conference, Uppsala, edited by C. M. Backman, T. Johannisson, and L. Tegner (Arkitektkopia, Uppsala, Sweden, 1982), p. 540.
[31]I. Rannou, Ph.D. thesis, Université Pierre et Marie Curie, 1984.
[32]H. D'Amour, W. B. Holzapfel, A. Polian, and A. Chevy, Solid State Commun. **44**, 853 (1982).
[33]H. Iwasaki, Y. Watanabe, N. Kuroda, and Y. Nishina, Physica B+C **105B**, 314 (1981).
[34]N. Kuroda, Y. Nishina, H. Iwasaki, and Y. Watanabe, Solid State Commun. **38**, 139 (1981).
[35]T. C. Chiang, J. Dumas, and Y. R. Schen, Solid State Commun. **28**, 173 (1978).
[36]V. Altshul, V. K. Bashenov, D. I. Marvakov, and A. G. Petukhov, Phys. Status Solidi B **98**, 715 (1980).
[37]A. Polian, M. Grimsditch, M. Fisher, and M. Gatulle, J. Phys. (Paris) Lett. **43**, L405 (1982).
[38]Y. Honma, M. Yamada, K. Yamamoto, and K. Abe, J. Phys. Soc. Jpn. **52**, 2777 (1983).
[39]M. Gatulle, M. Fisher, and A. Chevy, Phys. Status Solidi B **119**, 327 (1983).
[40]M. Gatulle and M. Fisher, Phys. Status Solidi B **121**, 59 (1984).
[41]T. J. Wieting, Solid State Commun. **12**, 931 (1973).
[42]S. Jandl, J. L. Brebner, and B. M. Powell, Phys. Rev. B **13**, 686 (1976).
[43]A. Polian, K. Kunc, R. Le Toullec, and B. Dorner, in *Proceedings of the 19th International Conference on the Physics of Semiconductors,* Inst. Phys. Conf. Ser. No. 43, edited by B. L. H. Wilson (IOP, London, 1979), p. 907.
[44]M. Piacentini, C. G. Olson, A. Balzarotti, R. Girlanda, V. Grasso, and E. Doni, Nuovo Cimento **54**, 248 (1979).
[45]F. Meyer, E. E. de Kluizenaar, and D. den Engelsen, J. Opt. Soc. **63**, 529 (1973).
[46]R. J. Elliott, Phys. Rev. **108**, 1384 (1957); in *Polarons and Excitons,* edited by C. G. Kuper and G. D. Whitefield (Plenum, New York, 1963), p. 269.
[47]Y. Toyozawa, Prog. Theor. Phys. **20**, 53 (1958); J. Phys. Chem. Solids **8**, 289 (1959); Prog. Theor. Phys. **27**, 89 (1962); J. Phys. Chem. Solids **25**, 59 (1964).
[48]R. Le Toullec, N. Piccioli, and J. C. Chervin, Phys. Rev. B **22**, 6162 (1980).
[49]M. Schlüter, Nuovo Cimento B **13**, 313 (1973).
[50]A. Bourdon, Ph.D. thesis, Université Pierre et Marie Curie, 1983.
[51]A. J. Niilisk and J. J. Kirs, Phys. Status Solidi **31**, K91 (1969).
[52]H. Kamimura, K. Nakao, and Y. Nishina, Phys. Rev. Lett. **22**, 129 (1969).
[53]A. Bourdon, M. Mejatty, R. Le Toullec, and J. M. Besson, in *Proceedings of the 13th International Conference on the Physics of Semiconductors,* edited by F. G. Fumi (Tipografia Marves, Rome, 1976), p. 1283.
[54]T. J. Wieting and J. C. Verble, Phys. Rev. B **5**, 1473 (1972).
[55]R. M. Hoff and J. C. Irwin, Can. J. Phys. **53**, 1606 (1975).
[56]B. A. Weinstein and G. J. Piermarini, Phys. Rev. B **4**, 1172 (1975).
[57]D. Petritis, G. Martinez, C. Levy-Clement, and O. Gorochov, Phys. Rev. B **23**, 6773 (1981).
[58]R. Zallen, Phys. Rev. B **9**, 4485 (1974).
[59]G. Martinez, in *Handbook on Semiconductors,* edited by J. S. Moss and M. Balkanski (North-Holland, Amsterdam, 1980), Vol. 2, p. 181.
[60]G. A. Samara, Phys. Rev. B **27**, 3494 (1983).
[61]B. A. Weinstein and R. Zallen, in *Light Scattering in Solids IV,* edited by M. Cardona and G. Güntherodt (Springer-Verlag, Berlin, 1984), p. 463.
[62]W. P. Dumke, M. R. Lorentz, and G. D. Pettit, Phys. Rev. B **5**, 2978 (1972).
[63]J. Gonzalez, Ph.D. thesis, Université Pierre et Marie Curie, 1988.
[64]N. Piccioli, R. Le Toullec, F. Bertrand, and J. C. Chervin, J. Phys. (Paris) **42**, 1129 (1981).
[65]Le Chi Thanh and C. Depeursinge, Solid State Commun. **21**, 317 (1977).
[66]N. Piccioli, Ph.D. thesis, Université Pierre et Marie Curie, 1987.
[67]J. Rigoult, J. Appl. Crystallogr. **12**, 116 (1979).
[68]N. M. Gasansly, B. M. Yavadov, V. I. Tagirov, and E. A. Vinogradov, Phys. Status Solidi B **89**, K43 (1978).
[69]L. N. Alieva, G. L. Belenkii, I. I. Reshina, E. Yu. Salaev, and V. Ya. Shteinshraiber, Fiz. Tverd. Tela (Leningrad) **21**, 155 (1980) [Sov. Phys.—Solid State **21**, 90 (1979)].
[70]S. Jandl, M. Banville, and J. Deslandes, Can. J. Phys. **59**, 198 (1981).
[71]J. Aidun, M. S. T. Bukowinski, and M. Ross, Phys. Rev. B **29**, 2611 (1984).
[72]J. C. Chervin, C. Andraud, N. Tercier, B. Blanzat, E. Cassanelli, and J. M. Besson, Phys. Rev. B **38**, 12 310 (1988).